Nanoscale

Accepted Manuscript

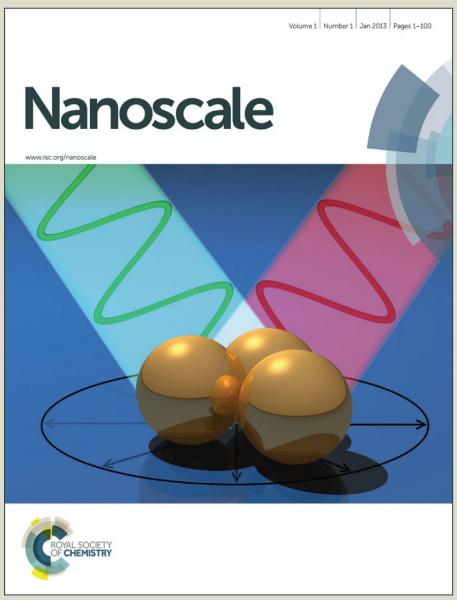

ROYAL SOCIETY OF CHEMISTRY

www.rsc.org/nanoscale

Journal Name

ARTICLE TYPE

Cite this: DOI: 10.1039/xxxxxxxxxx

CdSe/ZnS Quantum Dots as Sensors for the Local Refractive Index†

Antoine Aubret, Anne Pillonnet,* Julien Houel, Christophe Dujardin, and Florian Kulzer*

Received Date
Accepted Date

DOI: 10.1039/xxxxxxxxxx

www.rsc.org/journalname

We explore the potential of CdSe/ZnS colloidal quantum dots (QDs) as probes for their immediate dielectric environment, based on the influence of the local refractive index on the fluorescence dynamics of these nanoemitters. We first compare ensembles of quantum dots in homogeneous solutions with single quantum dots dispersed on various dielectric substrates, which allows us to test the viability of a conceptual framework based on a hard-sphere region-of-influence and the Bruggeman effective-medium approach. We find that all our measurements can be integrated into a coherent description, provided that the conceptualized point-dipole emitter is positioned at a distance from the substrate that corresponds to the geometry of the QD. Three theoretical models for the evolution of the fluorescence decay rate as a function of the local refractive index are compared, showing that the classical Lorentz approach (virtual cavity) is the most appropriate for describing the data. Finally, we use the observed sensitivity of the QDs to their environment to estimate the detection limit, expressed as the minimum number of traceable streptavidin molecules, of a potential QD-nanosensor based on fluorescence lifetime.

Introduction

The development of nanomaterials for biophotonics and biomedical applications has progressed at breathtaking pace in the last two decades, and nanoparticles can now be engineered to fulfill a great variety of diagnostic (sensing and imaging) as well as therapeutic functions[1–3]. Semiconductor quantum dots (QDs) are an important class of nanoparticles used in biomedical applications due to their favorable optical properties, including high emission quantum yields, large molar extinction coefficients comparable to those of organic dyes, broad absorption bands with narrow, symmetric photoluminescence (PL) spectra, large effective Stokes shifts, and resistance to photophysical and -chemical degradation[4–7]. The characterization and optimization of these properties or their uses as local probes has become a major interest during the last decades[8–11]. In particular, the ability to make water-soluble QDs and to target them to specific biomolecules has led to promising applications in cellular labeling and deep-tissue imaging[5,12]. Nanoparticles with a CdSe core in particular, which are readily available with a broad range of emission wavelengths in the visible spectral range, are widely used due to their photostability[13].

Among the various photophysical properties that can be exploited for sensing, the relaxation dynamics of nanoemitters are known to be a powerful tool for probing their immediate environment. For instance, Carlini *et al*. showed that lifetime imaging microscopy can elucidate the incorporation of QDs inside living cells and the concomitant changes in the QD oxidation state[14]. Furthermore, some experiments are able to deduce the quantum yield of ensemble[15] or single nanoemitters[16], suggesting applications as efficient single-photon sources and in other photonic devices[17].

Fundamentally, the relationship between the radiative transition probability γ_r of an emitter and the refractive index of its environment[18–21] is governed by Fermi's golden rule[22]:

$$\gamma_r = \frac{2\pi}{\hbar}\rho(\hbar\omega)|M|^2\delta_{E_2E_1} \quad (1)$$

Here, $\rho(\hbar\omega)$ is the density of states (DOS) of the electric field at frequency ω, E_2 and E_1 are, respectively, the energies of the initial and final states, and M is the matrix element of the dipolar-electric interaction Hamiltonian between the emitter and a local field. The influence of the medium manifests itself through the DOS and the local field, which in turn are directly related to the refractive index of the corresponding bulk material if the medium is homogeneous[21]. For emitters embedded in heterogeneous media, in particular in complex soft matter such as living cells, the question arises how the general principle embodied in Eq. (1) can be adapted to an effective-medium description based on a locally-defined refractive index that adequately reflects the influence of

Institut Lumière-Matière, CNRS UMR5306, Université Lyon 1, Université de Lyon, 69622 Villeurbanne CEDEX, France. Fax: +33 4 7243 1130; Tel: +33 4 7244 8347; E-mail: anne.pillonnet@univ-lyon1.fr, florian.kulzer@univ-lyon1.fr

† Electronic Supplementary Information (ESI) available: experimental techniques, further results and analysis. See DOI: 10.1039/b000000x/

the environment on the emission dynamics. Furthermore, as the refractive index has been shown to be a useful tool in the investigation of complex biochemical phenomena, such as the targeting of receptor molecules[23] or cell viability[24–26], it is important to understand over which characteristic distance R the environment exerts a noticeable influence on photophysical behavior of such nanoprobes. To elucidate these issues, we here show how the sensitivity of individual colloidal CdSe/ZnS core-shell QDs to their immediate environment can be used to measure the characteristic distance R over which a local effective refractive index can be conceptualized. To this end, we utilize a nanoscale effective medium approach to model the influence of the surrounding medium on γ_r and carry out a lifetime analysis on ensembles of QDs immersed in solutions of various refractive indices, as well as on single QDs deposited on different substrates. We furthermore discuss the potential of colloidal QDs as lifetime-based sensors of the local refractive index, and we compare the expected performance with that of sensors based on localized surface plasmon resonances (LSPR) of metallic nanoparticles.

Results and discussion

To test the applicability of an effective-medium description, we compared the fluorescence dynamics of QD525 and QD655 in solution to that observed for the same QD species on substrates with varying refractive indices. We will first discuss the decay curves measured for ensembles of quantum dots in solution, examples of which are shown in Figure 1. Different concentrations of sucrose in water were used to obtain solutions whose refractive indices varied between 1.33 and 1.46. Given that purification of QD samples by ultracentrifugation in sucrose solution can be carried out without loss of fluorescence[27], we assume that quenching by non-specific adsorption of sucrose molecules can be ruled out as a potential complication of our lifetime measurements, especially since the QDs we used are protected by a cross-linked polymer shell.

All fluorescence lifetime curves in this study were analyzed with a Poissonian maximum-likelihood estimator (MLE), which is, in contrast to the widely used χ^2-based fitting, efficient and unbiased,[28] especially for multiexponential decay curves with non-negligible background. (Details of all analysis methods are available in the ESI.) We found that all QD ensembles in solution exhibited a complex emission behavior that cannot be reproduced mono- or biexponential decay functions. In fact, the excited-state dynamics of CdSe/ZnS QDs are known to involve non-radiative relaxation channels as well as trap states, leading to multiexponential decay curves at the nanosecond timescale[29–32] and to power-law blinking over many orders of magnitude in time[33,34]. The states associated with the two decay rates in the biexponential lifetime curves of QDs are thought to be the neutral, highly emissive "on" state and the "off" (or "dim") state, a consequence of the ionization of the core of the nanocrystal. The latter phenomenon is known to open new non-radiative decay channels, thus lowering the luminescence quantum yield as compared to the on state[29–32]. Given that the typical integration time for a decay histogram in our experiments was around 100 s, each QD can be expected to have undergone many on/off transitions while it

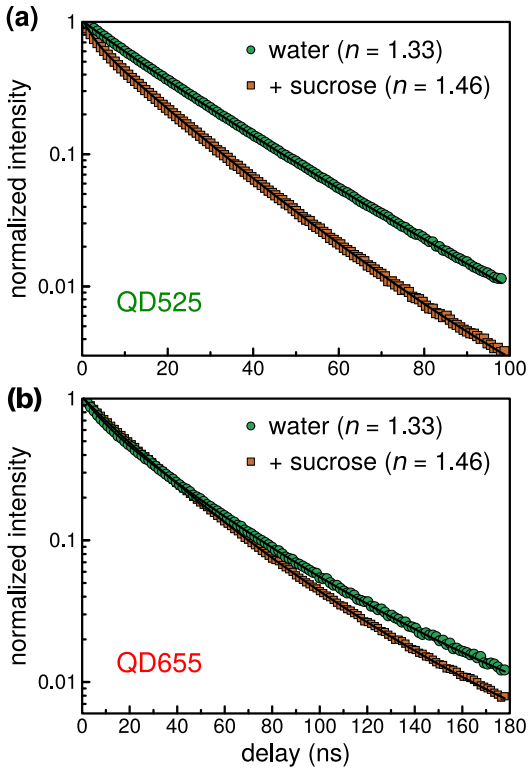

Fig. 1 Fluorescence dynamics of ensembles of QDs in solution, represented by the relative emission intensity as a function of the elapsed time after the exciting laser pulse. (a) Decay curves for QD525 in water ($n = 1.33$, circles) and in sucrose solution ($n = 1.46$, squares). The solid lines correspond to fits of biexponential decay curves with a Gaussian distribution of both rates, yielding $\gamma_1 = 0.0489\,\mathrm{ns}^{-1}$ in water and $\gamma_1 = 0.0648\,\mathrm{ns}^{-1}$ in the sucrose solution. (b) Decay curves for QD655 in water ($n = 1.33$, circles) and in a sucrose solution ($n = 1.46$, squares). The solid lines correspond to the same fits as in (a), now yielding $\gamma_1 = 0.0259\,\mathrm{ns}^{-1}$ in water and $\gamma_1 = 0.0323\,\mathrm{ns}^{-1}$ in the sucrose solution.

was investigated. Both neutral and charged states thus contribute to all decay curve, resulting in the presence of a slow (γ_1) and a fast ($\gamma_2 > \gamma_1$) component, which correspond to luminescence photons emitted during the "on" and "off" periods, respectively. (The "off"/"dim" state has a significantly lower, but non-zero emission rate.) We note that recent experiments indicate that the interplay between blinking and luminescence lifetime is more complicated than suggested by the model outlined above[32], especially for CdSe/CdS QDs[35,36]. Nevertheless, the present study deals with modeling the dynamics of the single-exciton radiative process as a point-dipole in an effective medium; consequently we focus exclusively on the slow rate (γ_1) in the following discussion. Furthermore, to allow for the size and shape inhomogeneities within the QD ensembles measured in solution, we introduced Gaussian distributions[30,37] around the central decay rates of the on- and off-states, γ_1 and $\gamma_2 > \gamma_1$, respectively. The corresponding standard deviations of the distributions, σ_1 (on-state) and σ_2 (off-state), for any given solution turned out to be 20% for QD525 and 30% for QD655. A clear variation of γ_1 with the refractive index of the solution was observed, as can be appreciated from the two limiting cases shown in Figure 1. (Please refer to the ESI for

further details of the MLE fitting procedure and tables of all rates γ_i and standard deviations σ_i.) Typically, the contribution of the fast component (γ_2) was on the order of, at most, a few percent of the total number of detected luminescence photons, which means that the fast process does not interfere with the accurate determination of the on-state component γ_1.

Three different theoretical models are commonly employed to predict the radiative relaxation rate as a function of the refractive index of the surrounding medium. The virtual cavity model (VC)[38] was first developed by Lorentz for dilute gases. This classical model introduces a cavity as a conceptual separation between the continuous dielectric and the discrete point-dipole at its center; the cavity is virtual in the sense that it is still "filled" with the dielectric material. The second model, developed by Glauber and Lewenstein in 1990, adopts a quantum point of view and is known as the empty cavity model (EC)[39] (or Onsager model or real cavity model). Here, a normal mode expansion of the field in the dielectric allows to derive an expression for γ_{rad} of an emitter in the center of a cavity that is considered to be empty. The third model is the fully microscopic one (FM) of Crenshaw and Bowden[40]. This last model considers the interactions between the emitter and the atoms of the dielectric medium (treated as two-level systems) at the microscopic level to find an approximated (first-order) solution for the equation of motion of the excited state of the emitter. The resulting expressions for the radiative depopulation rate γ_{r} as a function of the effective refractive index $\bar{n}$ are

$$\gamma_{1\mathrm{r}}(\bar{n}) = \begin{cases} \left(\frac{\bar{n}^2+2}{3}\right)^2 \bar{n}\,\gamma_{1\mathrm{rv}} & \text{for the VC model} \\ \left(\frac{3\bar{n}^2}{2\bar{n}^2+1}\right)^2 \bar{n}\,\gamma_{1\mathrm{rv}} & \text{for the EC model} \\ \frac{\bar{n}^2+2}{3}\,\gamma_{1\mathrm{rv}} & \text{for the FM model} \end{cases}, \qquad (2)$$

where $\gamma_{1\mathrm{rv}} = \gamma_{1\mathrm{r}}(\bar{n}=1)$ is the radiative decay rate in vacuum. The predicted increase of $\gamma_{1\mathrm{r}}$ with increasing refractive index is most pronounced for the VC model, less strong for the EC model and weakest for the FM model.

We have applied these three models to our data, using as free parameters the radiative decay rate in vacuum $\gamma_{1\mathrm{rv}}$ and the non-radiative decay rate $\gamma_{1\mathrm{nr}}$ (assumed to be independent of $\bar{n}$). The expression to fit to our data thus takes the form $\gamma_1 = \gamma_{1\mathrm{nr}} + \gamma_{1\mathrm{r}}(\bar{n})$, where $\gamma_{1\mathrm{r}}(\bar{n})$ is given by Eq. (2). As can be seen in Figure 2a, the EC and FM models fail to reproduce the data of QD525 because they both underestimate the influence of the medium on the decay rate, even for the absence of non-radiative relaxation, *i.e.*, for a luminescence quantum yield of 100%. Only the virtual cavity model is able to reproduce the experimental data from QDs in solutions over the full range of indices, finding vacuum quantum yields of 0.87 and 0.67 for QD525 and QD655, respectively. These values agree well with Duan *et al.*[41], who reported similar quantum yields for the same types of QDs in the framework of the VC model. We note that the FM model was successfully employed in earlier measurements of QD fluorescence lifetimes in organic solvents which were carried out by Wuister *et al*[19]. However, the FM model has been criticized from a fundamental point

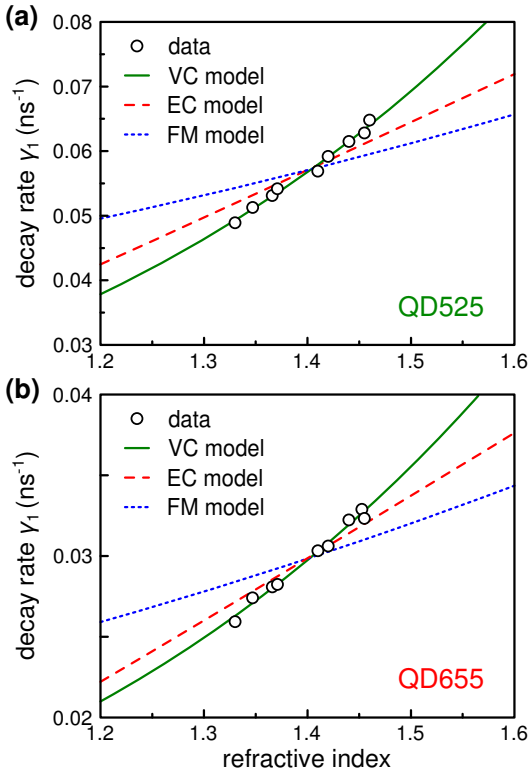

Fig. 2 The fluorescence dynamics of QD525 and QD655 in solutions with refractive indices between 1.33 and 1.46. (a) Mean on-state decay rate (center of Gaussian distribution) γ_1 of QD525 (open circles, error bars smaller than symbols) as a function of the refractive index of the solutions. Fits of the data according to the VC (solid line), EC (dashed line), and FM (dotted line) models are shown over a larger range of refractive indices to accentuate the difference between the models. (b) Fluorescence dynamics of QD655 in solution, data points and fits analogous to (a).

of view, given that it predicts anisotropic refractive indices for perfectly isotropic media. This criticism is derived from a refined microscopic model put forth by Berman and Milonni[42], which takes into account sub-magnetic levels of the atoms in the environment; the improved model furthermore shows that both the VC and the EC approach are consistent with it for dilute gases ($n \to 1$), while the FM approach predicts a different slope at $n = 1$ for the curve of $\gamma_{1\mathrm{r}}$ as a function of n. These calculations were extended by Fu and Berman in 2005 to the second order for a simplified Hamiltonian[43], which finally allows to distinguish between the VC and the EC model, thus showing that only the VC approach remains consistent with the refined microscopic model. Furthermore, a theoretical comparison published by Crenshaw in 2008[44] likewise concluded that microscopic theory of quantum electrodynamics is in agreement with the classical approach to local-filed correction, *i.e.*, the VC model. The experimental results of the present work confirm the inadequacy of both the EC and the FM model, at least for the QD525 species, while for the analogous QD655 data (ellipsoid QDs), Figure 2b, only the FM model can be ruled out. For the sake of completeness, we furthermore point out that derivatives of the EC model have recently been shown to describe the environment-dependent emission dy-

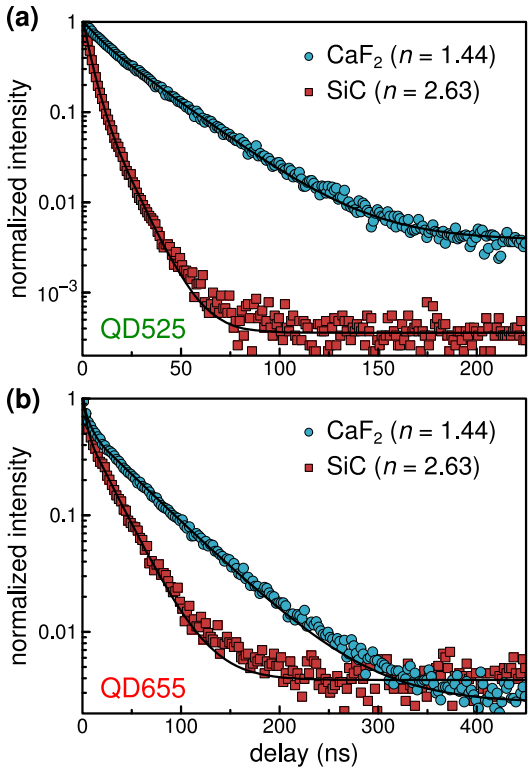

Fig. 3 Fluorescence dynamics of single QDs on substrates, represented by the relative emission intensity as a function of the elapsed time after the exciting laser pulse. (b) Decay curves of an individual QD525 particle on a CaF_2 substrate ($n = 1.436$, circles) and of another QD525 on a SiC substrate ($n = 2.672$, squares). The solid lines correspond to a biexponential decay model, from which we obtained values of $\gamma_1 = 0.0353\,\mathrm{ns}^{-1}$ (CaF_2) and $\gamma_1 = 0.0989\,\mathrm{ns}^{-1}$ (SiC), respectively, for these particular decay curves. (b) Decay curves as in (a) but now for two QD655 particles, one on CaF_2 ($n = 1.433$, circles) and the other one on SiC ($n = 2.629$, squares). Biexponential decay models (solid lines) yield $\gamma_1 = 0.0180\,\mathrm{ns}^{-1}$ (CaF_2) and $\gamma_1 = 0.0367\,\mathrm{ns}^{-1}$ (SiC), respectively.

namics of other types of emitters, such as Ce^{3+} and Tb^{3+} ions in $LaPO_4$ crystals[45].

The values of γ_1 in solution, *i.e.*, a homogeneous medium, will serve as a reference for an effective medium approach to model the relaxation dynamics of the same QDs on various dielectric substrates. In particular, it will allow us to demonstrate how an effective refractive index $\bar{n}$ has to be calculated in the latter situation so that the observed decay rates are in agreement with the decay rates in a homogeneous solution of the same refractive index. Examples of decay curves of the two QD species can be seen in Figure 3 for the two substrates corresponding to the minimum and maximum refractive indices explored in the present study; as discussed above, the decay histograms are expected to have two components γ_1 and γ_2 corresponding to on- and off-state emission, respectively, which was indeed found to be the case for all measurements of QDs on substrates. However, as we are now dealing with individual emitters, there is no need for introducing a distribution of decay rates as was the case for the ensembles measured in solution. Repeating the lifetime measurement on different QDs for each type of substrate yielded a mean value of the on-state decay rate and its empirical standard deviation. (We did verify that decay histograms constructed from photons emitted during "on" periods showed the expected mono-exponential decay with rate γ_1, see ESI for details.) The observed distribution of the decay rate γ_1 for QDs of the same species investigated on the same substrate is attributed to a distribution of sizes and shapes, but also to differences in the orientation of the emitting dipole with respect to the surface of the substrate. Lukosz[46] has shown for an emitter close to a plane dielectric discontinuity that an orientation-dependent modification of the local density of states (LDOS) occurs, which affects the luminescence rate and the emission diagram. Special care was therefore taken in our experiments to select single QDs with a wide range of luminescence intensities, so that the resulting mean value of γ_1 represents, as closely as possible, an average over all possible orientations of the dipole on the surface, as well as a sampling of potential shape heterogeneity at the single-QD level.

Our interpretation of the changes in decay rate γ_1 induced by the environment is based on the calculation of an effective refractive index surrounding the emitter, for characterizing the absolute value of the decay rate. The different materials in the volume over which the emitter is sensitive to the environment are taken into account *via* the Bruggeman effective medium approach[47], which avoids the often somewhat arbitrary distinction between "host" and "guest" components in a mixed medium; instead, it treats each constituting phase equally as an inclusion in the effective medium itself (see ESI for details). A limiting distance can be introduced beyond which the influence of the medium becomes negligible, be it as a cut-off radius R or by a smoothly decaying weighting function to quantify how the influence of the environment diminishes with its distance from the emitter. The simplest possible model for this distance dependence is that of a hard sphere, which establishes a sharp boundary by assuming that only the dielectric material within a sphere of radius R centered on the emitter contributes (uniformly) to $\bar{n}$, as is illustrated in Figure 4a. We have previously applied such a hard-sphere model to the luminescence dynamics of the same QD species sandwiched between two dielectric interfaces whose distance varied due to a spherical-planar contact geometry[48], for which we found that the QD decay rate decreased with increasing distance of the second interface until a cut-off distance on the order of 80 nm was reached. With regard to interpreting the substrate data of the present study, we note that conceptualizing the emissive transition as an electric point-dipole will necessarily neglect the geometry of the QDs and the finite extension of the exciton, but it remains important to take into account the size of the nanoparticle when deciding where this point-dipole has to be localized relative to the substrate surface, see Figure 4a. Figure 4b compares the γ_1 decay rates of QD525 in solution (cf. Figure 2a) to those found on the substrates; the top panel represents the naive calculation of the effective refractive index for the latter cases based on a point dipole located directly at the surface of the substrate. It can be seen clearly that no agreement between the two experiments can be achieved in this case. It should be noted that this result is independent of the cut-off radius R of the effective index calculation because the volume fraction of the substrate is always 50% of a total interaction sphere centered on the surface.

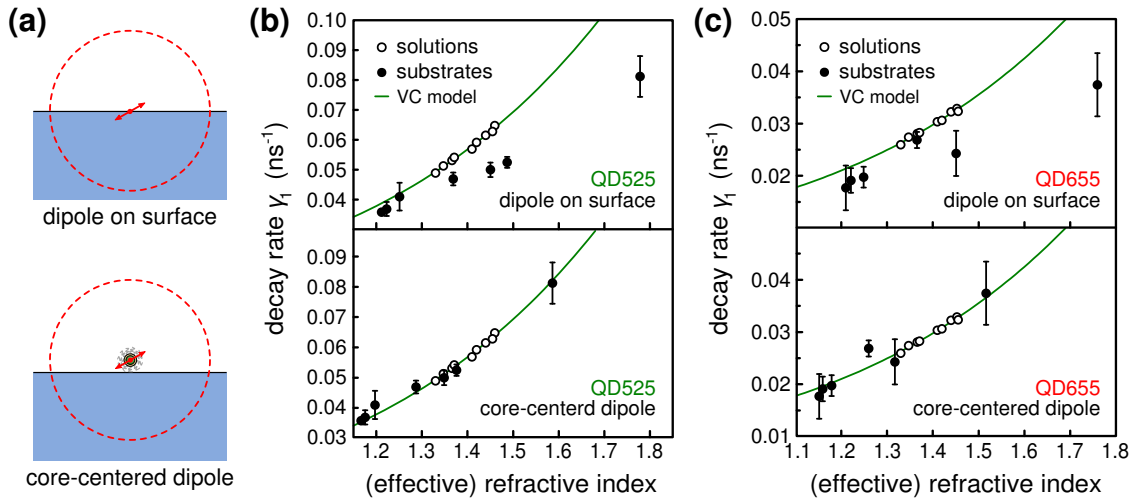

Fig. 4 Effective-medium description of the influence of the dielectric environment on the relaxation dynamics of optically-excited quantum dots. The effective refractive index $\bar{n}$ for the substrate measurements is calculated using the Bruggeman effective medium theory in a hard-sphere of radius R around point-dipole-like emitter. (a) In the dipole-on-surface scheme (top), the point-dipole is envisioned to rest directly on the substrate surface, in which case $\bar{n}$ is independent of R. On the other hand, the emitting dipole is positioned at a distance from the surface that corresponds to the QD geometry in the core-centered dipole approach (bottom). (b) The fluorescence dynamics of QD525: The open circles represent ensemble measurements in solutions with refractive indices between 1.33 and 1.46. (This is the same data as in Fig. 2a, whose error bars are smaller than the symbols.) The full circles show average rates for QDs studied individually on various dielectric substrates; error bars denote the empirical standard deviations of each ensemble. The effective refractive index for the substrate measurements is calculated under the dipole-on-surface assumption (top) and the core-centered dipole scheme with $R = 44$ nm for QD525 and $R = 50$ nm for QD655 (bottom), respectively. The solid line represents the best fit of γ_1 in solution as a function of $\bar{n}$ according to the virtual cavity (VC) model, which is the only one able to reproduce the data. (c) The fluorescence dynamics of QD655, data and interpretation analogous to (b).

On the other hand, positioning the point-like emitter – and thus the center of the interaction sphere – at a distance from the surface that corresponds to the radius of the core/shell/polymer QD structure (~ 6 nm for QD525 and ~ 9 nm for QD655) allows for an agreement between the two experiments: In this core-centered dipole geometry, the radius of the interaction sphere remains as the only free parameter to adjust for maximum overlap of the substrate data points with the VC model derived from the solution measurements, see Figure 4bc; the optimum radius was thus found to be $R = (44 \pm 4)$ nm for QD525 and $R = (50 \pm 8)$ nm for QD655. These two values of the critical radius are smaller than those found in the aforementioned earlier investigations (~ 80 nm)[48] for comparable QDs. We attribute the discrepancy to secondary effects that may have been present in the earlier experiments, for example mechanical strain at the sphere-substrate contact point and a possible influence of the polymer adhesion layer that was used. Furthermore, the values of the present study are more reliable due to the higher number of photons in the decay histograms and the ML analysis.

Having quantified the response of QD525 to changes in the effective refractive index of a nanoscale volume, we can now compare the expected performance of a QD525-based sensor to that of plasmonic nanoprobes. The latter variety of nanosensor relies on the local surface plasmon resonance (LSPR) of metallic particles; gold in particular is widely used in the form of nanorods, -ellipsoids, -prisms, -stars, and other shapes[49–53]. The LSPR frequency changes with the refractive index of the surrounding medium, which allows detection of analyte molecules in ultra-low concentrations ($\lesssim$ zeptomolar) without chemical amplification[54–58]. A useful figure of merit (FoM) to quantify the performance of LSPR nanoprobes in this kind of application is the frequency shift per refractive index unit (RIU), relative to the full width at half maximum (FWHM) of the plasmonic absorption band[59]. However, we note that the sensing volume of QD525, a sphere with a radius of (44 ± 4) nm in our effective medium description, is significantly larger than the effective sensing volume of a plasmonic nanosensor, whose interaction with the environment decreases exponentially over characteristic lengths of $10-20$ nm[60–62]. The reduced sensing volume works in of favor plasmonic nanosensors because the same refractive index sensitivity achieved over a smaller volume means that a smaller absolute quantity of an analyte can be detected. For a fair and meaningful comparison, we therefore adopt the formalism of Nusz *et al.*[57], which takes into account the role for the sensing volume in overall performance. Adapting Eq. (6) of Ref. 57 to a potential QD525-based refractive index nanosensor, we obtain

$$\frac{\Delta\gamma_1}{\Delta n \cdot S} = \frac{V_\mathrm{d}}{V_\mathrm{s}} \quad , \tag{3}$$

which assumes that the observed change in the on-state fluorescence decay rate, $\Delta\gamma_1$, is proportional to the volume occupied by the detected analyte, V_d, divided by the total sensing volume V_s. If the sensing volume is completely filled by the analyte so that $V_\mathrm{d}/V_\mathrm{s} = 1$, then $\Delta\gamma_1$ is given by the product of Δn, the difference in refractive index between the analyte and the pure (analyte-free) solution, and the sensitivity S of the sensor, expressed in ns^{-1}/RIU. As we base our considerations on a hard-sphere model, S is independent of r, the distance between a given

analyte molecule and the sensor's surface, which means that all analyte molecules within V_s are given equal weight in contributing to $\Delta\gamma_1$.

For an analyte molecule of known molecular volume V_m, the volume occupied by N detected molecules is given by $V_d = N \cdot V_m$. Furthermore, after determining the minimum change $\delta\gamma_1$ of the decay rate that can be resolved under given experimental conditions, one can estimate the corresponding minimum number of detectable analyte molecules, N_{lim}, according to

$$N_{lim} = \frac{\delta\gamma_1}{\Delta n \cdot S} \cdot \frac{V_s}{V_m} \quad . \tag{4}$$

The sensitivity S of QD525 can be derived from the data of Figure 1a: A modification of the refractive index n from 1.33 to 1.46 induces a change of the average γ_1 from $0.0489\,ns^{-1}$ to $0.0648\,ns^{-1}$, which means that the sensitivity is $S = 0.122\,ns^{-1}/RIU$. Still following Ref. 57, we consider streptavidin as a model analyte, with a molecular volume of $V_m = 114\,nm^3$ and a bulk refractive index of $n = 1.57$, leading to $\Delta n = 1.57 - 1.33 = 0.24$ RIU for a sensor operating in aqueous solution. The remaining two parameters needed to estimate the detection limit according to Eq. (4) are the sensing volume V_d and the experimental accuracy of the on-state decay rate, $\delta\gamma_1$. The latter contribution is the dominant source of uncertainty for the potential application that we consider here, which entails the detection of only a limited number of photons emitted by a single nanoparticle. To ensure a realistic value for N_{lim}, we choose a conservative upper limit of 50 nm for the radius of the hard-sphere sensing volume, which leads to $V_d = 5.2 \cdot 10^5\,nm^3$, after subtracting the volume occupied by core, shell and polymer layer of QD525 ($r = 6$ nm). Finally, $\delta\gamma_1$ was estimated from the uncertainty in γ_1 when fitting the expected decay function to the data of an individual QD525 particle on BK7. We found that the best accuracy was obtained when the photon counting histogram was constructed from on-state photons, which were selected by applying a threshold criterion to binned timetraces; the decay functions were found to be strictly mono-exponential in this case (see ESI). Constructing the decay histogram from increasingly longer parts of single-particle timetraces allowed us to explore the dependence of $\delta\gamma_1$ on the number of analyzed photons; representative values are $\delta\gamma_1 = 1.4 \cdot 10^{-4}\,ns^{-1}$ for hundred thousand photons and $\delta\gamma_1 = 5.5 \cdot 10^{-5}\,ns^{-1}$ for a million of them. The decay rates were determined from maximum-likelihood analysis for a mono-exponential probability density with constant background, combined with the bootstrap method (see ESI) to estimate the uncertainty $\delta\gamma_1$.

Eq. (4) predicts detection limits N_{lim} of several tens of streptavidin molecules; as shown in Figure 5, one finds the expected $1/\sqrt{N_{phot}}$ behavior, where N_{phot} is the number of detected photons. The limiting value achieved with the highest number of photons is less than 10 molecules for a photon number higher than one million. We note that if the background cannot be determined from an independent measurement then it has to be introduced as an additional fit parameter, which reduces the achievable accuracy to an estimated detection limit of ~ 18 molecules for one million photons. These values are comparable to the detection limit

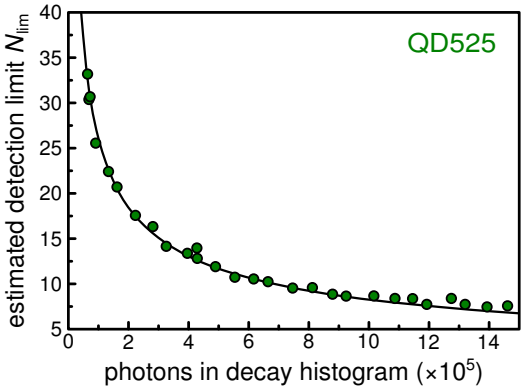

Fig. 5 The estimated detection limit of a single QD525 nanosensor, quantified by the minimum detectable number N_{lim} of streptavidin molecules in the detection volume, as a function of the number of photons that are accumulated to construct the fluorescence decay histogram. The points are calculated from the experimentally observed uncertainties $\delta\gamma_1$ in the determination of the on-state decay rate γ_1 and the solid line is a fit of a $N_{lim} \propto 1/\sqrt{N_{phot}}$ relationship, where N_{phot} is the number of photons.

of 18 – 22 molecules that Nusz *et al.*[57] find for plasmonic sensors based on a gold nanorods with optimized dimensions. However, the potential QD525-based sensor that we discuss here requires longer integration times of around 700 seconds to achieve this performance, although this duration can probably be reduced by at least a factor of ten if the excitation intensity is increased, especially if highly-emissive, photostable and non-blinking QDs[63] are used. We therefore think our proposed scheme might find applications, for example in combination with methods for rapid lifetime measurements[64] and in cases where the considerably larger size or the shorter sensitivity range (which may require a higher analyte concentration) of plasmonic sensors is undesirable. Finally, for interpreting data from QD-based sensors relying on a more specific interaction with a functionalized nanoparticle surface, the results presented here may be useful to incorporate the unspecific "baseline" sensitivity into the analysis, which stems from refractive index changes due to the presence of the analyte or other species.

Conclusions

We have investigated the influence of the local dielectric environment on the fluorescence emission dynamics of colloidal CdSe/ZnS quantum dots. Comparing the luminescence lifetimes in an isotropic, homogeneous medium with the ones found after deposition on a dielectric interface, we could show that an interpretation in terms of a point-dipole emitter embedded in an effective medium requires taking into account the non-zero size of the QDs and introducing a characteristic distance R over which an effective refractive index is calculated. We found a value of $R \approx 45$ nm for the hard sphere model combined with the Bruggeman effective medium approach, which may help to judge the region of influence when QDs are employed as nanoprobes in lifetime imaging and related techniques. Furthermore, we are able to discriminate between three models commonly used to quantify the relationship between emission dynamics and the refractive

index of the surrounding medium; in agreement with recent theoretical advances we presented experimental evidence in favor of the virtual cavity model, with plausible values of the fluorescence quantum yield ranging from 0.87 in vacuum to 0.96 on a SiC substrate. Finally, a comparison with plasmonic nanoparticles shows that single colloidal QDs, especially recently developed highly emissive ones, might have a comparable potential as nanosensors for refractive index, whose performance may complement plasmonic nanosensors for certain applications.

Experimental section

Fluorescent Quantum Dots

We used water-soluble CdSe/ZnS core-shell colloidal quantum dots (Invitrogen, ITK carboxyl quantum dots, Q21341MP and Q21321MP) emitting at 525 nm (QD525) and at 655 nm (QD655). These nanoparticles contain a cadmium selenide core that is capped by a zinc sulfide shell to improve chemical and optical properties. A final polymer shell is added around the QD, which is important for the retention of the optical properties and to allow facile dispersion of the QDs in aqueous solutions. In particular, the surrounding medium can then be modified without changing the exciton non-radiative decay rate. The diameters of the core/shell structures are about 3.5 nm for the nearly spherical QD525, and around 12 nm by 6 nm (maximum and minor axis) of the ellipsoidal QD655 species. The overall radii R of the emitters including the polymer layer are $R_{\mathrm{QD525}} = 6\,\mathrm{nm}$ and $R_{\mathrm{QD655}} = 9\,\mathrm{nm}$ according to the manufacturer.

Ensemble Lifetime Measurements in Solution

Comparison measurements were conducted on ensembles of quantum dots in homogeneous solutions of different refractive indices. A stock solution of 20% (weight) sucrose in distilled water was heated under stirring to 50 °C in a water bath so that evaporation gradually increased the sucrose concentration. Samples of 1 ml were taken at various stages of the evaporation process and their refractive index was measured in an Abbe refractometer after thermalization to room temperature. We thus had access to a range of solutions whose refractive index varied between 1.33 (pure water) and 1.46 (about 70% sucrose). Drops of 10 μl of either QD525 or QD655 solution at $c = 10^{-6}$ mol/l were added to the 1 ml samples to achieve final QD concentrations $c = 10^{-8}$ mol/l.

The relaxation dynamics of the QDs in the different solutions were measured in a setup that is schematically shown in Figure S1c of the ESI: A picosecond pulsed laser diode (Hamamatsu, M10306-31) emitting at 444 nm with a repetition rate of 1 MHz was used at excitation powers well below saturation and focused into the solution by a 150 mm lens. The emitted luminescence was collected at 90 ° by a 50 mm lens and focused onto the cathode of a photomultiplier tube (Picoquant, PMA-C-165-N-M) after spectral filtering. The pulses of the photomultiplier were processed by time-correlated single photon counting electronics (Picoquant, PicoHarp 300) to build the decay histogram from the photon arrival times relative to the exciting laser pulses with a nominal resolution of 32 ps and an overall instrumental response function IRF with a width of 0.4 ns.

Lifetime Measurements of Single QDs

The relaxation dynamics of individual quantum dots were analyzed on seven different substrates: calcium fluoride (CaF_2, refractive index $n = 1.436$ at 525 nm), Suprasil (synthetic fused SiO_2, $n = 1.460$), borosilicate glass (BK7, $n = 1.520$), aluminum oxide (Al_2O_3, $n = 1.772$), yttrium aluminum perovskite (YAP, $n = 1.950$), lanthanum dense flint (LASF, $n = 2.030$), and silicon carbide (6H-SiC, $n = 2.672$). In the case of SiC, the 6H polytype was chosen because it has no absorption bands overlapping with the emission of either QD species, which rules out potential complications due to energy transfer from the QDs to the SiC substrate. QDs were dispersed on these substrates by depositing a drop (10-20 μl) of an aqueous solution of either QD525 or QD655 at a concentration of $c = 10^{-8}$ mol/l on and spin-coating for 120 seconds at 2000 rotations per minute (RPM) with an acceleration of 200 RPM/s. We thus obtained samples with a suitably low surface coverage to allow observation of individual QDs by a home-built confocal microscope (see Figure S1a of the ESI) capable of time-correlated single photon counting. QDs were excited with 200 fs laser pulses centered around 446 nm at repetition rates that could accommodate the emitters' relaxation dynamics between two successive pulses (4 MHz for QD525 and 2 MHz for QD655). Time-correlated single photon counting (TCSPC) electronics (Picoquant, TimeHarp 200) allowed to record the arrival times of all detected photons relative to the laser pulses with an internal temporal resolution better than 40 ps and an overall instrumental response function (IRF) whose width was about 0.6 ns.

Acknowledgements

We thank D. Carole for the SiC substrates and C. Belacel, G. Ledoux, and D. Amans for discussions. This work was supported by the Programme Avenir Lyon Saint-Étienne (ANR-11-IDEX-0007) of Université de Lyon, within the program "Investissements d'Avenir" operated by the French National Research Agency (ANR). Technical support of the Lyon Center for Nano-Opto Technologies (NanOpTec) is gratefully acknowledged. This work was performed in the context of the European COST Action MP1302 Nanospectroscopy.

References

1 J. L. West and N. J. Halas, *Annu. Rev. Biomed. Eng.*, 2003, **5**, 285–292.
2 M. De, P. S. Ghosh and V. M. Rotello, *Adv. Mater.*, 2008, **20**, 4225–4241.
3 B. Mu, J. Q. Zhang, T. P. McNicholas, N. F. Reuel, S. Kruss and M. S. Strano, *Accounts Chem. Res.*, 2014, **47**, 979–988.
4 A. P. Alivisatos, W. W. Gu and C. Larabell, *Annu. Rev. Biomed. Eng.*, 2005, **7**, 55–76.
5 I. L. Medintz, H. T. Uyeda, E. R. Goldman and H. Mattoussi, *Nat. Mater.*, 2005, **4**, 435–446.
6 R. C. Somers, M. G. Bawendi and D. G. Nocera, *Chem. Soc. Rev.*, 2007, **36**, 579–591.

7 D. A. Wheeler and J. Z. Zhang, *Adv. Mater.*, 2013, **25**, 2878–2896.

8 H. M. Fan, Z. H. Ni, Y. P. Feng, X. F. Fan, J. L. Kuo, Z. X. Shen and B. S. Zou, *Appl. Phys. Lett.*, 2007, **90**, 021921.

9 Z. Li, L. Wang, B. B. Liu, J. H. Wang, B. Liu, Q. J. Li, B. Zou, T. Cui, Y. Meng, H. K. Mao, Z. X. Liu and J. Liu, *Phys. Status Solidi B-Basic Solid State Phys.*, 2011, **248**, 1149–1153.

10 P. A. S. Jorge, C. Maule, A. J. Silva, R. Benrashid, J. L. Santos and F. Farahi, *Anal. Chim. Acta*, 2008, **606**, 223–229.

11 E. Betzig, G. H. Patterson, R. Sougrat, O. W. Lindwasser, S. Olenych, J. S. Bonifacino, M. W. Davidson, J. Lippincott-Schwartz and H. F. Hess, *Science*, 2006, **313**, 1642–1645.

12 J. M. Costa-Fernandez, R. Pereiro and A. Sanz-Medel, *TracTrends Anal. Chem.*, 2006, **25**, 207–218.

13 P. Guyot-Sionnest, *C. R. Phys.*, 2008, **9**, 777–787.

14 L. Carlini and J. L. Nadeau, *Chem. Commun.*, 2013, **49**, 1714–1716.

15 P. Lunnemann, F. T. Rabouw, R. J. A. van Dijk-Moes, F. Pietra, D. Vanmaekelbergh and A. F. Koenderink, *ACS Nano*, 2013, **7**, 5984–5992.

16 X. Brokmann, L. Coolen, M. Dahan and J. P. Hermier, *Phys. Rev. Lett.*, 2004, **93**, 107403.

17 S. Buckley, K. Rivoire and J. Vučković, *Rep. Prog. Phys.*, 2012, **75**, 126503.

18 G. Lamouche, P. Lavallard and T. Gacoin, *Phys. Rev. A*, 1999, **59**, 4668–4674.

19 S. F. Wuister, C. D. Donega and A. Meijerink, *J. Chem. Phys.*, 2004, **121**, 4310–4315.

20 C. Tregidgo, J. A. Levitt and K. Suhling, *J. Biomed. Opt.*, 2008, **13**, 031218.

21 D. Toptygin, *J. Fluoresc.*, 2003, **13**, 201–219.

22 E. Fermi, *Rev. Mod. Phys.*, 1932, **4**, 87–132.

23 H. J. van Manen, P. Verkuijlen, P. Wittendorp, V. Subramaniam, T. K. van den Berg, D. Roos and C. Otto, *Biophys. J.*, 2008, **94**, L67–69.

24 C. L. Curl, C. J. Bellair, T. Harris, B. E. Allman, P. J. Harris, A. G. Stewart, A. Roberts, K. A. Nugent and L. M. D. Delbridge, *Cytom. Part A*, 2005, **65A**, 88–92.

25 N. Pavillon, J. Kuhn, C. Moratal, P. Jourdain, C. Depeursinge, P. J. Magistretti and P. Marquet, *PLoS One*, 2012, **7**, e30912.

26 J. Park, S. Il Jin, H. M. Kim, J. Ahn, Y. G. Kim, E. G. Lee, M. G. Kim and Y. B. Shin, *Biosens. Bioelectron.*, 2015, **64**, 241–246.

27 O. Carion, B. Mahler, T. Pons and B. Dubertret, *Nat. Protoc.*, 2007, **2**, 2383–2390.

28 J. Kim and J. Seok, *Opt. Express*, 2013, **21**, 6061–6075.

29 G. Schlegel, J. Bohnenberger, I. Potapova and A. Mews, *Phys. Rev. Lett.*, 2002, **88**, 137401.

30 B. R. Fisher, H. J. Eisler, N. E. Stott and M. G. Bawendi, *J. Phys. Chem. B*, 2004, **108**, 143–148.

31 D. Ratchford, K. Dziatkowski, T. Hartsfield, X. Q. Li, Y. Gao and Z. Y. Tang, *J. Appl. Phys.*, 2011, **109**, 103509.

32 A. A. Cordones, T. J. Bixby and S. R. Leone, *Nano Lett.*, 2011, **11**, 3366–3369.

33 R. Verberk, J. W. M. Chon, M. Gu and M. Orrit, *Physica E*, 2005, **26**, 19–23.

34 F. Cichos, C. von Borczyskowski and M. Orrit, *Curr. Opin. Colloid Interface Sci.*, 2007, **12**, 272–284.

35 C. Galland, Y. Ghosh, A. Steinbruck, M. Sykora, J. A. Hollingsworth, V. I. Klimov and H. Htoon, *Nature*, 2011, **479**, 203–75.

36 C. Galland, Y. Ghosh, A. Steinbruck, J. A. Hollingsworth, H. Htoon and V. I. Klimov, *Nat. Commun.*, 2012, **3**, 908.

37 C. Belacel, B. Habert, F. Bigourdan, F. Marquier, J. P. Hugonin, S. M. de Vasconcellos, X. Lafosse, L. Coolen, C. Schwob, C. Javaux, B. Dubertret, J. J. Greffet, P. Senellart and A. Maitre, *Nano Lett.*, 2013, **13**, 1516–1521.

38 J. Knoester and S. Mukamel, *Phys. Rev. A*, 1989, **40**, 7065–7080.

39 R. J. Glauber and M. Lewenstein, *Phys. Rev. A*, 1991, **43**, 467–491.

40 M. E. Crenshaw and C. M. Bowden, *Phys. Rev. Lett.*, 2000, **85**, 1851–1854.

41 C. K. Duan, M. F. Reid and Z. Q. Wang, *Phys. Lett. A*, 2005, **343**, 474–480.

42 P. R. Berman and P. W. Milonni, *Phys. Rev. Lett.*, 2004, **92**, 053601.

43 H. Fu and P. R. Berman, *Phys. Rev. A*, 2005, **72**, 022104.

44 M. E. Crenshaw, *Phys. Rev. A*, 2008, **78**, 053827.

45 T. Senden, F. T. Rabouw and A. Meijerink, *ACS Nano*, 2015, **9**, 1801–1808.

46 W. Lukosz and R. E. Kunz, *J. Opt. Soc. Am.*, 1977, **67**, 1607–1615.

47 D. E. Aspnes, *Am. J. Phys.*, 1982, **50**, 704–709.

48 A. Pillonnet, P. Fleury, A. I. Chizhik, A. M. Chizhik, D. Amans, G. Ledoux, F. Kulzer, A. J. Meixner and C. Dujardin, *Opt. Express*, 2012, **20**, 3200–3208.

49 A. J. Haes, D. A. Stuart, S. M. Nie and R. P. Van Duyne, *J. Fluoresc.*, 2004, **14**, 355–367.

50 A. J. Haes and R. P. Van Duyne, *Anal. Bioanal. Chem.*, 2004, **379**, 920–930.

51 K. A. Willets and R. P. Van Duyne, *Annu. Rev. Phys. Chem.*, 2007, **58**, 267–297.

52 S. Lal, S. Link and N. J. Halas, *Nat. Photonics*, 2007, **1**, 641–648.

53 K. Saha, S. S. Agasti, C. Kim, X. N. Li and V. M. Rotello, *Chem. Rev.*, 2012, **112**, 2739–2779.

54 A. D. McFarland and R. P. Van Duyne, *Nano Lett.*, 2003, **3**, 1057–1062.

55 N. Nath and A. Chilkoti, *Anal. Chem.*, 2004, **76**, 5370–5378.

56 C. Novo, A. M. Funston, I. Pastoriza-Santos, L. M. Liz-Marzan and P. Mulvaney, *J. Phys. Chem. C*, 2008, **112**, 3–7.

57 G. J. Nusz, A. C. Curry, S. M. Marinakos, A. Wax and A. Chilkoti, *ACS Nano*, 2009, **3**, 795–806.

58 O. Kedem, A. Vaskevich and I. Rubinstein, *J. Phys. Chem. C*, 2014, **118**, 8227–8244.

59 L. J. Sherry, S. H. Chang, G. C. Schatz, R. P. Van Duyne, B. J.

Wiley and Y. N. Xia, *Nano Lett.*, 2005, **5**, 2034–2038.
60 J. Schmitt, P. Mächtle, D. Eck, H. Möhwald and C. A. Helm, *Langmuir*, 1999, **15**, 3256–3266.
61 T. Okamoto, I. Yamaguchi and T. Kobayashi, *Opt. Lett.*, 2000, **25**, 372–374.
62 A. J. Haes, S. L. Zou, G. C. Schatz and R. P. Van Duyne, *J. Phys. Chem. B*, 2004, **108**, 6961–6968.
63 B. Mahler, P. Spinicelli, S. Buil, X. Quélin, J. P. Hermier and B. Dubertret, *Nat. Mater.*, 2008, **7**, 659–664.
64 Y. Won, S. Moon, W. Yang, D. Kim, W. T. Han and D. Y. Kim, *Opt. Express*, 2011, **19**, 3396–3405.